Heliyon 6 (2020) e04689

Contents lists available at ScienceDirect

Heliyon

journal homepage: www.cell.com/heliyon

Review article

Series solution of unsteady MHD oblique stagnation point flow of copper-water nanofluid flow towards Riga plate

Rizwana Rizwana [a], Azad hussain [a,*], S. Nadeem [b,c]

[a] Department of Mathematics, University of Gujrat, Gujrat, Pakistan
[b] Mathematics and its Applications in Life Sciences Research Group, Ton Duc Thang University, Ho Chi Minh City, Viet Nam
[c] Faculty of Mathematics and Statistics, Ton Duc Thang University, Ho Chi Minh City, Viet Nam

ARTICLE INFO

Keywords:
Mechanical engineering
Riga plate
Vacillating plate
Non-Newtonian nanofluid flow
Fixed frame
Series solution
Two phase flow model

ABSTRACT

This article concentrates on the non-Newtonian fluid flow over the oscillating surface. The rate of heat conduction of the fluid is enhanced by taking nanofluids in it. The two-phase nanofluid flow model is revealed. The flow is explored in the existence of oblique stagnation point flow. The analysis is incorporated for the Riga plate in the existence of an oblique stagnation point. Riga plate is well-known as an electromagnetic actuator contains permanent magnets and a spanwise aligned array of alternating electrodes attached on a plane surface. The dimensional equations satisfying the stated assumptions of the fluid flow are presented utilizing the Navier-Stokes equation. Fourier law is incorporated in the evaluation of heat flux. The analysis is examined in the fixed frame of reference. The obtained partial differential equation will be critically examined suitable similarity transformation will be chosen to convert these flow developed equations into higher non-linear ordinary differential equations (ODE) and these equations of motion are tackled by mathematical techniques like bvp4c method in Maple. From this study, it is determined that due to the effect of the Riga parameter the velocity field enhances, and also due to the effects of Casson parameter the velocity field increases. The effect of immerging of parameters is mentioned by tables and graphs. Moreover, the flow behavior is also confirmed by streamlines. The Casson fluid parameter makes to get faster the fluid velocity. The system heats up by the impact of Joule heating and dissipation.

1. Introduction

The analysis of nanofluids is getting to obtain the attention of investigators due to superior thermal conductivity and wide applications in the engineering and industrial purposes like microscale and macro heat transfer, transportation and biomedicine, nuclear reactors, etc., given by Choi et al. [1]. Nanofluids have filled the usual convection of a two-dimensional cavity. Hoghoughi, G et al. [2] explored various models that are compared by the physical properties of nanofluids. The nano liquid discoveries beneficial applications in manufacturing, cooling of electronic devices, heat exchangers, transportation, paints, biomedicine. Yu, Q., et al. [3] explored the nanofluids are predictable to be used in current engineering problems involving into polymerase chain reaction efficiency, solar collectors, radiators, and electronic cooling system. A vital source of thermal characteristics and natural convection fluid flow is associated with buoyancy driven flows contained by an enclosure explored by Purusothaman et al. [4]. A similar investigation has been conducted by many researchers [5,6,7].

In current years, non-Newtonian fluids are often encountered in numerous industrial and physical progressions because the analyses of non-Newtonian fluids have been inspired expressively. Frequent fluids treated as non-Newtonian fluids including drilling mud, clay coating, paints, fruit squash, shampoos, polymer fluxes, blood, and certain oils, etc. Shen [8] demonstrated that as compared to Newtonian fluid flow, the constitutive performance of non-Newtonian fluid flow is normally more complex. According to their physical behavior, the non-Newtonian fluids are divided into many branches one of the important branches is Casson fluid or shear-thinning fluids. For this type of fluids, the visible viscosity displays declining manners against applied shear stress. The mutual and vital illustration of such fluid is human blood is given by Khan et al. [9]. In the current past, many investigators have been contributed to the research of non-Newtonian fluid [7,10].

The fluid motion occurs on all compact bodies moving in a fluid known as stagnation point flows. The stagnation region encounters the maximum rates of mass deposition, the maximum heat transfers, and the uppermost pressure explored by Heimans et al. [11]. Stagnation point

* Corresponding author.
E-mail address: azad.hussain@uog.edu.pk (A. hussain).

https://doi.org/10.1016/j.heliyon.2020.e04689
Received 8 October 2019; Received in revised form 31 January 2020; Accepted 7 August 2020

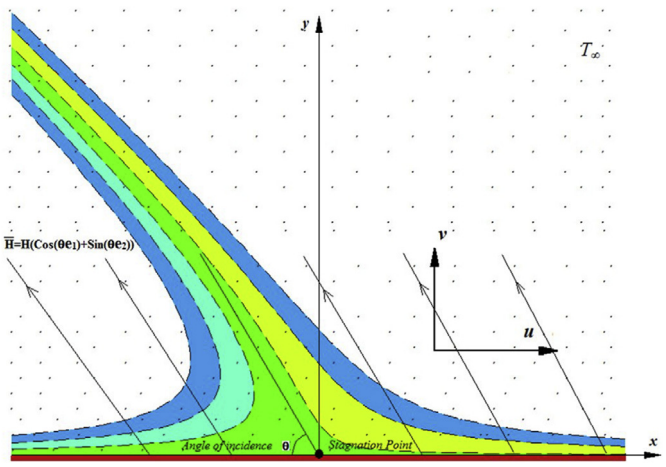

Figure 1. Physical intention of the flow problem.

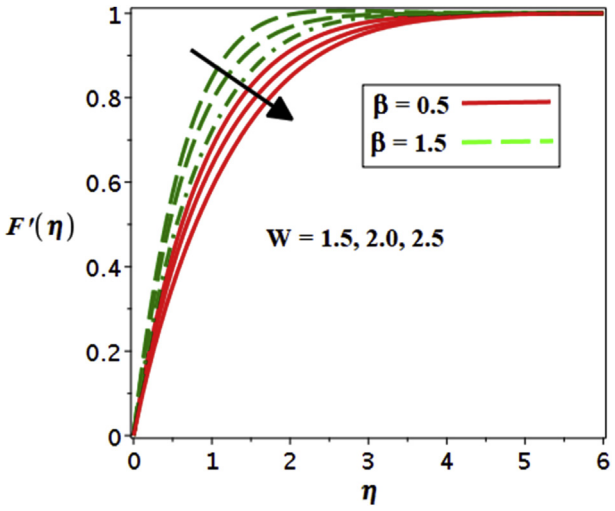

Figure 2. Impression of W on $F^{'}(\eta)$.

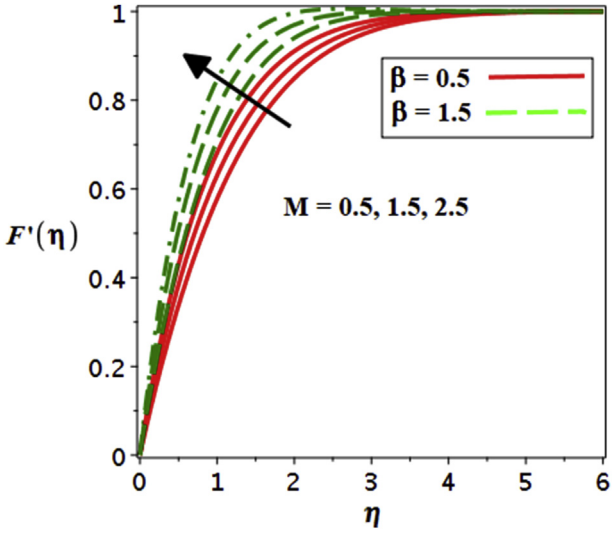

Figure 3. Result of β on $F^{'}(\eta)$.

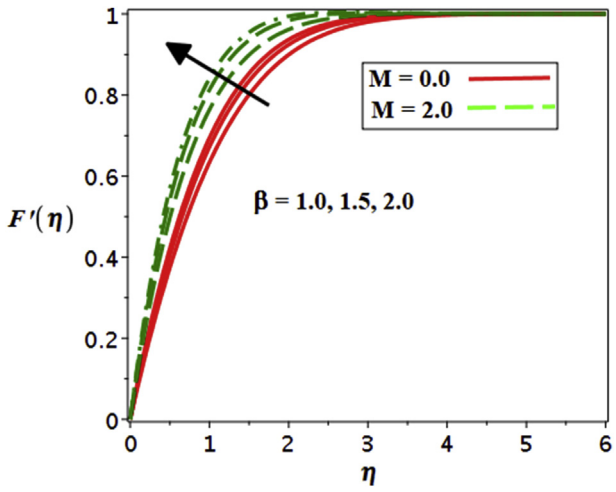

Figure 4. Result of M on $F^{'}(\eta)$.

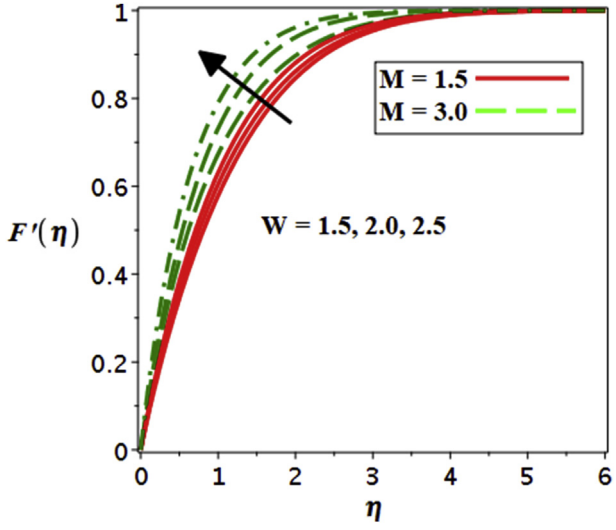

Figure 5. Result of w on $F^{'}(\eta)$.

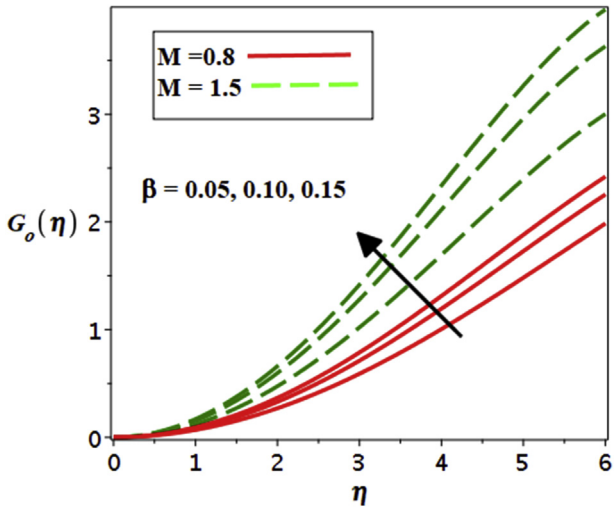

Figure 6. Impact of M and β on velocity Component $G_o(\eta)$.

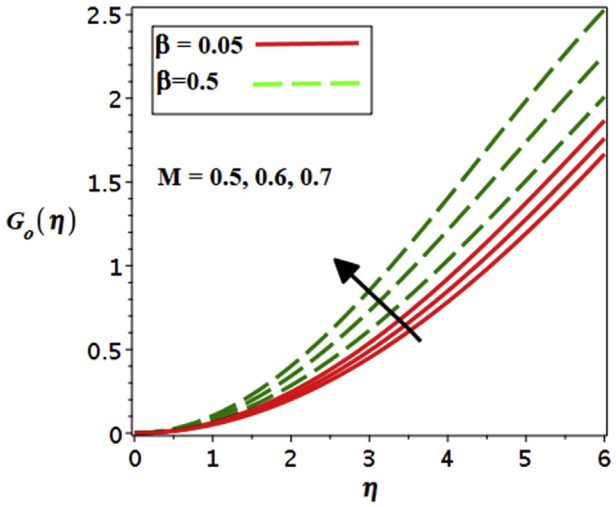

Figure 7. Effect of β and M on velocity component $G_o(\eta)$.

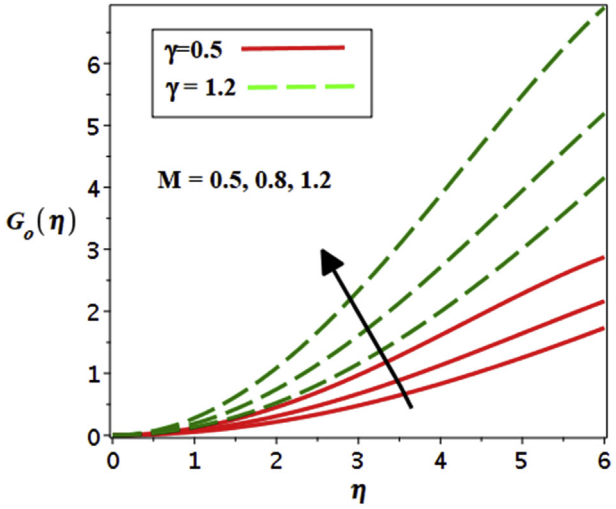

Figure 8. Inspiration of γ and M on $G_o(\eta)$.

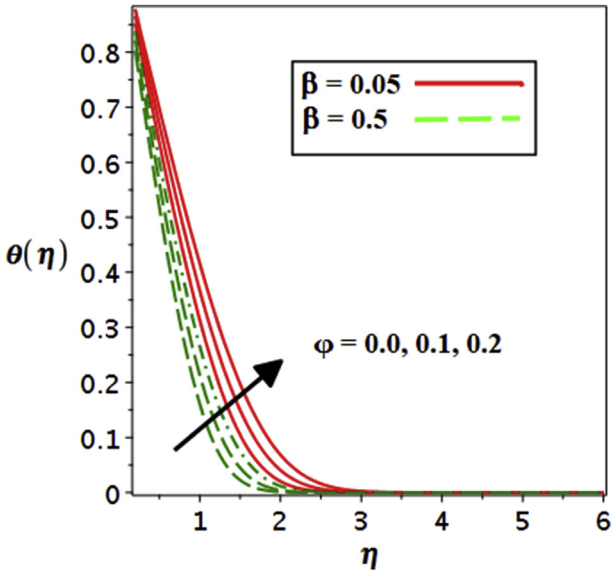

Figure 9. Result of ϕ and β on temperature.

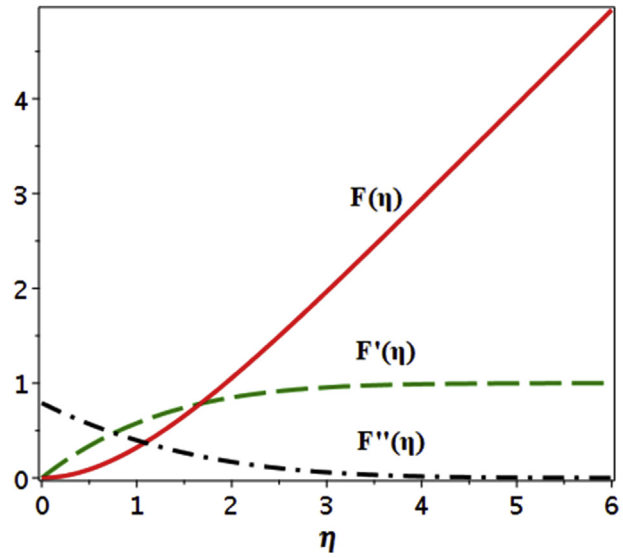

Figure 10. Plots exposing $f(\eta)$, $f'(\eta)$, $f''(\eta)$for $M = 1.5$, $\beta = 0.5$, $\gamma = 0.5$.

flows with heat flow facet are fairly apparent in crystal puffing, paper manufacture, revolving fibers, melt spinning process, and continuous molding given by Mehmood et al. [12]. In the prediction of skin-friction moreover, heat transfer or mass transfer close stagnation areas of bodies in great speed movements, radial diffusers, drag decline, the project of thrust compartment, transpiration cooling, drag decrease, and thermal oil repossession the stagnation point flow with several physical possessions has great physical significance given by S. Nadeem et al. [13]. Such kind of topic has been studied by researchers [14,15,16].

The magnetic field holds a significant place in fluid mechanics due to the sophisticated improvement in the thermophysical properties of a fluid. Astrology and field like earth science use these fluids which proved to be poor electric conductors. Therefore, an external agent is suggested to improve conductivity via the heat transfer process and related thermophysical characteristics. A magnetic bar can be that external agent or maybe permanently fixed magnets with alternate electronics. Such as experiment was first carried out by Gailitis and Lielausis et al. [17]. Ahmad et al. [18] report laminar fluid over the Riga plate which is supported by theoretically that this efficient agent reduces skin friction. Some fruitful research has been studied on this topic [19,20,21,22,23,24,25,26,27].

The current study analysis uses the fixed frame of reference and non-Newtonian fluid with the two-phase flow model on the oscillating plate.

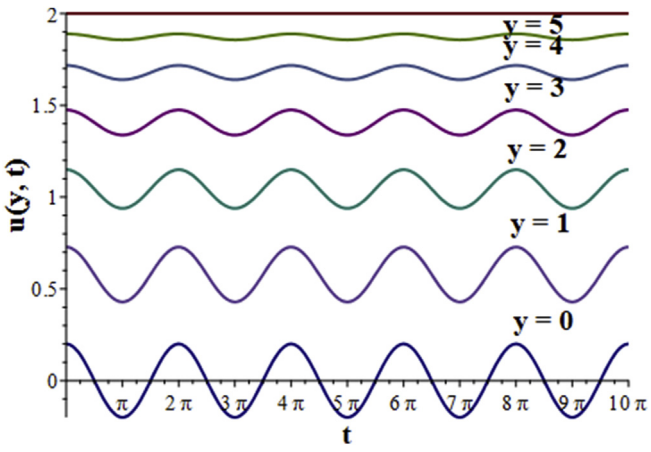

Figure 11. Time dependent flow.

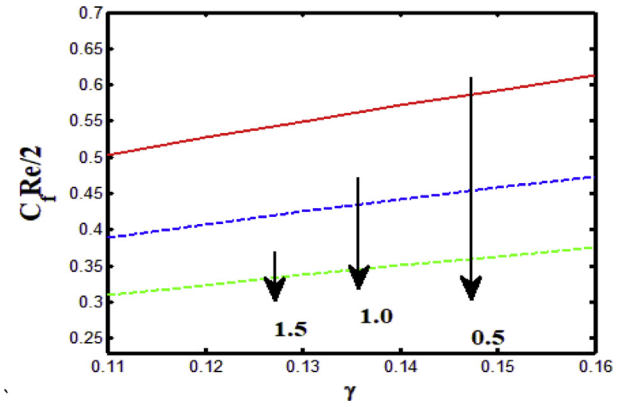

Figure 12. The consequence of M and γ on Skin friction.

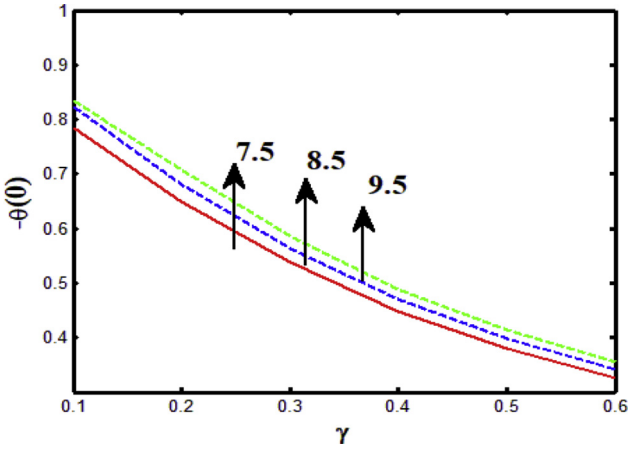

Figure 13. Deviation of Pr and ϕ on Nusselt number.

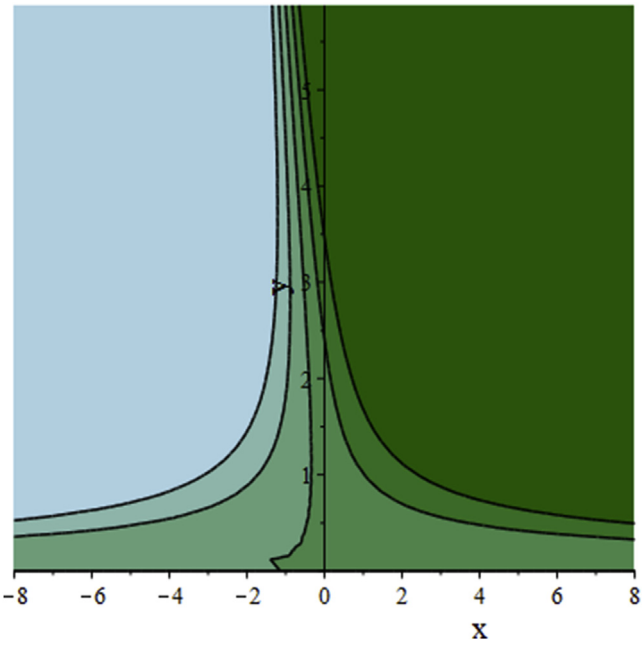

Figure 15. Stream lines for $\beta = 2$.

Heat transfer is shown for Cu nanoparticles. It is perceived that the occurrence of Cu nanoparticles reduces the Skin friction coefficient whereas heat transfer develops. The Casson fluid parameter makes to get faster the fluid velocity. The partial differential equations for vacillating 2D flows are simplified in a fixed frame by considering the supposed form of solutions. The coupled differential equations are tackled by a mathematical technique like the bvp4c method in maple. The influence of several parameters such as Casson parameter, Riga parameter, Hartmann Number on skin friction, temperature, and velocity profile. Moreover, flow performance is also demonstrated by streamlines.

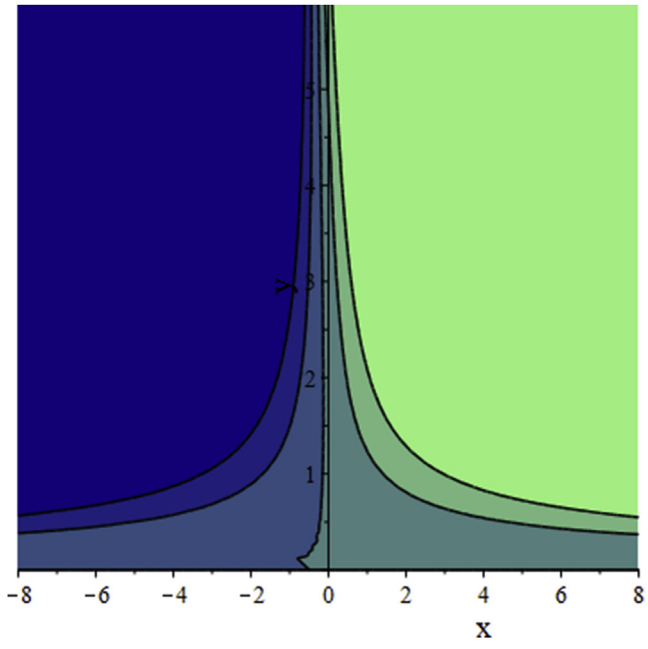

Figure 14. Stream lines for $\beta = 1$.

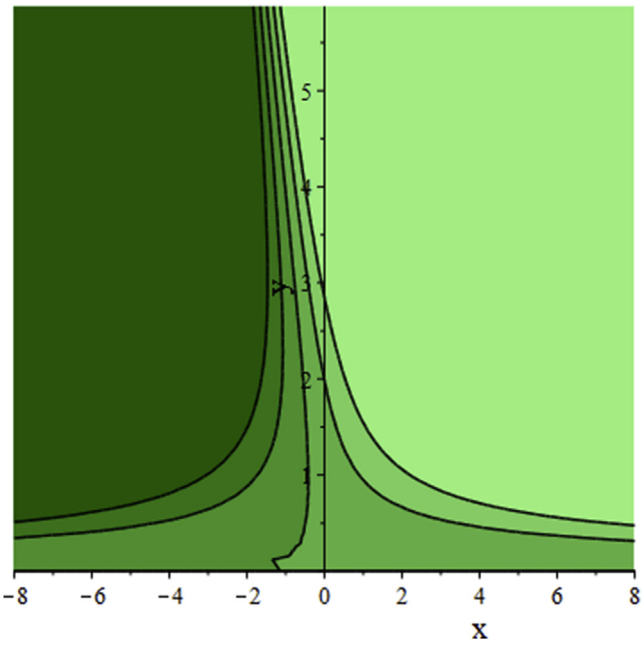

Figure 16. Stream lines for $\beta = 3$.

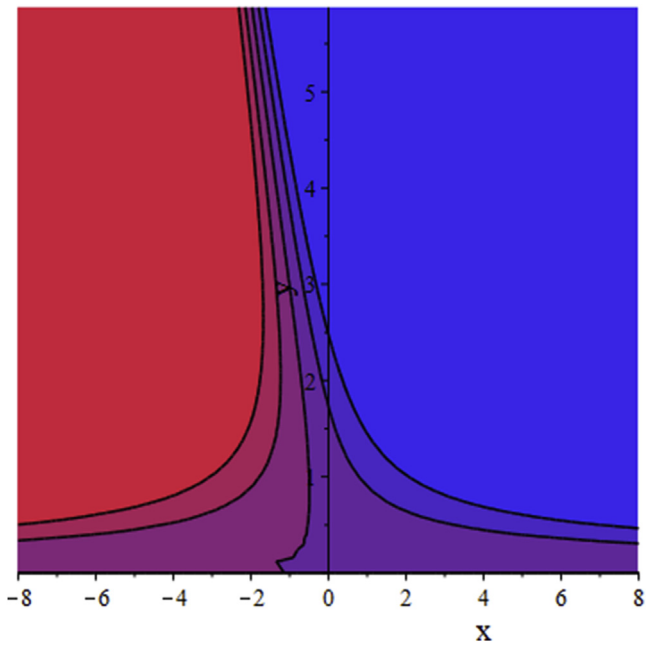

Figure 17. Stream lines for $\beta = 4$.

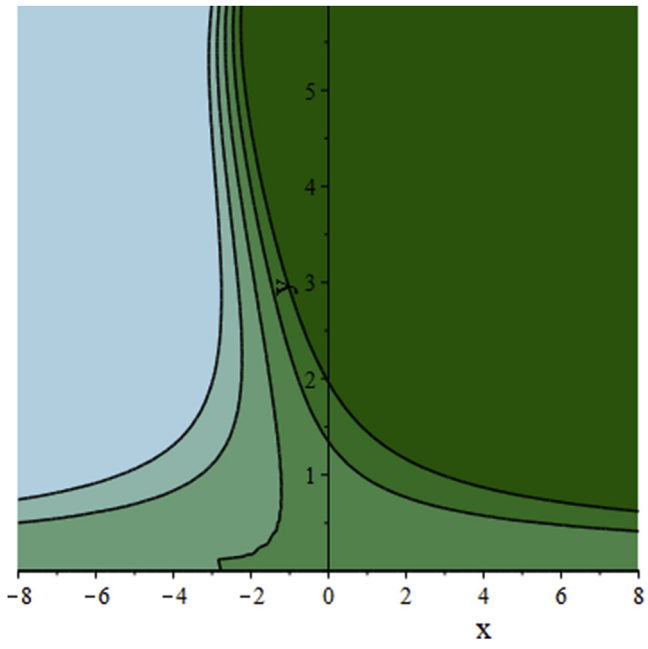

Figure 19. Stream lines for $M = 4$.

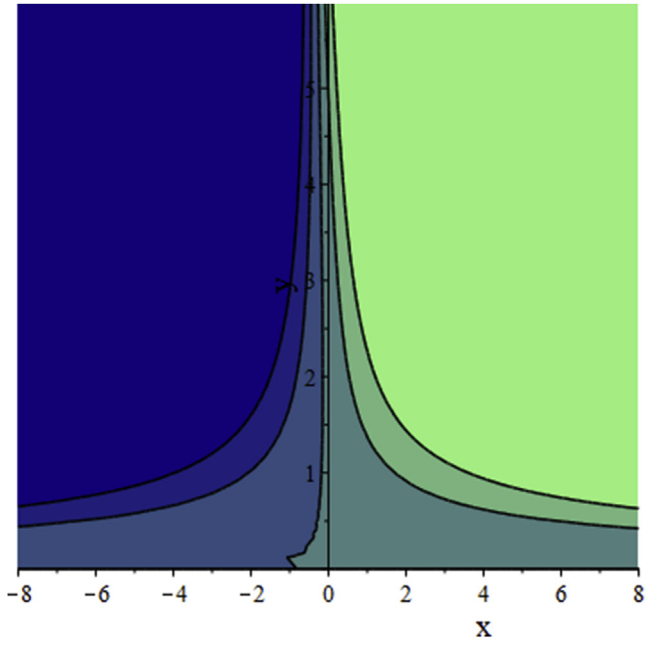

Figure 18. Stream lines for $M = 2$.

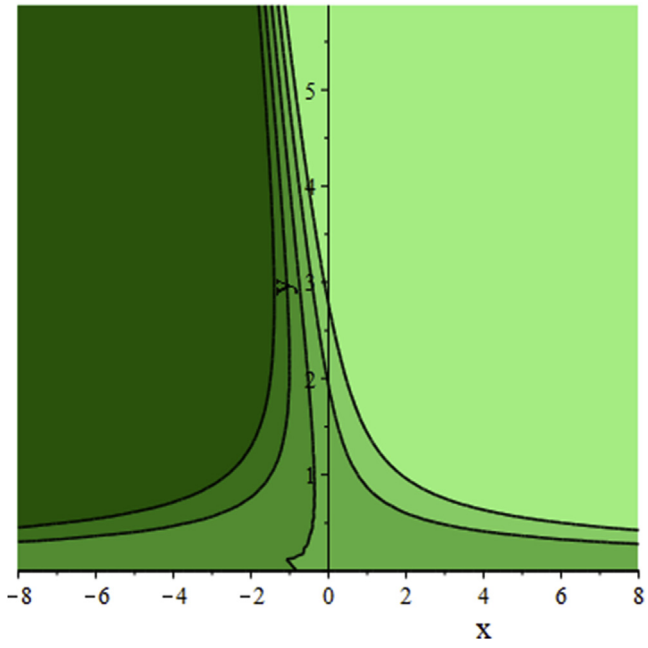

Figure 20. Stream lines for $M = 6$.

2. Mathematical equations for non-Newtonian fluid flow

Consider two-phase flow model for non-Newtonian fluid with Riga plate, unsteady, incompressible state flow. The plate vacillating in its own plan and the flow of the nanofluid distract obliquely on it. The fluid is in the upper half of the plane $y \geq 0$. The equations are defined as

$$\tau_{ij} = -p_{ij} + \left\{ \begin{array}{ll} 2\left[u_B + \frac{p_y}{\sqrt{2\pi}}\right] eij & \pi > \pi_c \\ 2\left[u_B + \frac{p_y}{\sqrt{2\pi_c}}\right] eij & \pi_c > \pi \end{array} \right\}, \tag{1}$$

$$\frac{\partial u}{\partial x} + \frac{\partial v}{\partial y} = 0, \tag{2}$$

$$\frac{\partial u}{\partial t} + u\frac{\partial u}{\partial x} + v\frac{\partial u}{\partial y} = \nu_{nf}\left(1 + \frac{1}{\beta}\right)\left(\frac{\partial^2 u}{\partial x^2} + \frac{\partial^2 v}{\partial y^2}\right) - \frac{1}{\rho}\frac{dp}{dx} + \frac{\pi J_0 M_0}{8\rho_f}\exp\left(-\frac{\pi}{a}y\right), \tag{3}$$

$$\frac{\partial v}{\partial t} + u\frac{\partial v}{\partial x} + v\frac{\partial v}{\partial y} = \nu_{nf}\left(1 + \frac{1}{\beta}\right)\left(\frac{\partial^2 u}{\partial x^2} + \frac{\partial^2 v}{\partial y^2}\right) - \frac{1}{\rho}\frac{dp}{dx}, \tag{4}$$

$$\alpha_{nf}\left(\frac{\partial^2 T}{\partial y^2} + \frac{\partial^2 T}{\partial x^2}\right) = u\frac{\partial T}{\partial x} + v\frac{\partial T}{\partial y} + \frac{\partial T}{\partial t}. \tag{5}$$

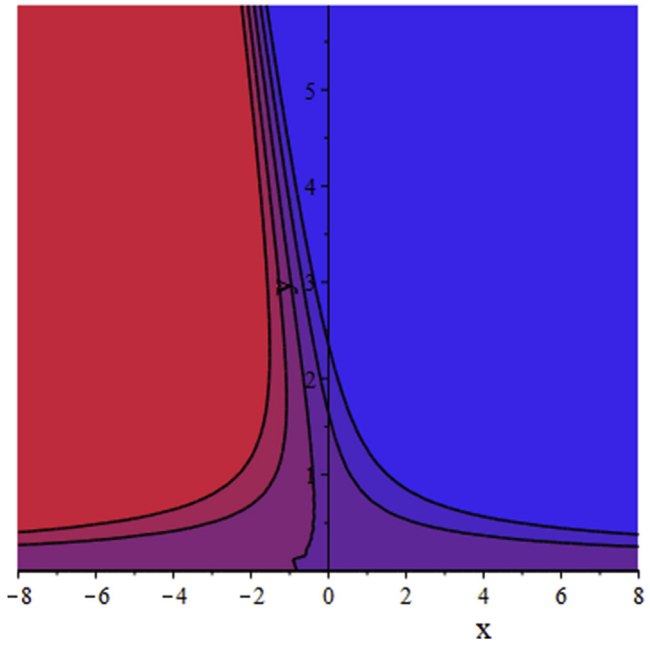

Figure 21. Stream lines for $M = 8$.

Where j_o is the current density width of magnetic, electrodes is a and M_o the magnetization of permanent magnets.

The continuity Eq. (1) implies the occurrence of a stream function ψ like as

$$u = \frac{\partial \psi}{\partial y}, \quad v = -\frac{\partial \psi}{\partial x}. \tag{6}$$

Implementing the Eq. (6) on Eqs. (3), (4), and (5) and eliminate the pressure using $p_{xy} = p_{yx}$, yields

$$\nu_{nf}\left(1+\frac{1}{\beta}\right)(\nabla^4\psi) + \frac{\partial(\psi, \nabla^2\psi)}{\partial(x,\ y)} - \frac{\pi J_0 M_0}{8\rho_f}\frac{\partial}{\partial y}\exp\left(-\frac{\pi}{a}y\right) - \frac{\partial(\nabla^2\psi)}{\partial t} = 0, \tag{7}$$

$$\alpha_{nf}\left(\frac{\partial^2 T}{\partial y^2} + \frac{\partial^2 T}{\partial x^2}\right) - \frac{\partial \psi}{\partial y}\frac{\partial T}{\partial x} - \frac{\partial T}{\partial t} + \frac{\partial \psi}{\partial x}\frac{\partial T}{\partial y} = 0. \tag{8}$$

3. Fixed frame of reference for the phase flow model

Conferring to [16] we consider that

$$\psi = k[xf(y) + g(y)], \tag{9}$$

where k is a parameter. We examine that about the plate is oscillating at the point $y = 0$, and the fluid engaged at the upper half plane $y > 0$. The

Table 1. The impact of γ and M on Skin friction coefficient.

γ	M	$\frac{1}{2}C_f R_e = F'(0) + F''(0)$
0.1	0.1	-0.839302
0.11		- 0.937015
0.12		-1.053934
0.1	0.1	-0.829415
	0.2	-0.933832
	0.3	-1.026499

Table 2. The impact of γ and Pr on Nusselt number.

γ	Pr	$-\theta(\eta)$
0.1	7.5	0.674924
0.12		0.831899
0.14		1.082955
0.1	7.5	0.665935
	8.5	0.857260
	9.5	0.888969

flow function is given by [16], $\psi = \frac{1}{2}\gamma y^2 + xy$. The boundary conditions are given below

$$\begin{aligned} g(y) = 0, \quad g_y(y) = 0, \quad f(y) = 0, \quad f'(y) = 0, \quad at\ y = 0, \\ g_y(y) = \gamma y, \quad f'(y) = 1, \quad as\ \ y \to \infty. \end{aligned} \tag{10}$$

Where the γ is dimensionless and implementing (9) on (7), we obtain

$$\nu_{nf}\left(1+\frac{1}{\beta}\right)\left(\frac{d^4 f}{dy^4}\right) - \frac{\pi J_0 M_0}{8\rho_f}\frac{\partial}{\partial y}\exp\left(-\frac{\pi}{a}y\right) + k\left(f\frac{d^3 f}{dy^3} - \frac{df}{dy}\frac{d^2 f}{dy^2}\right) = 0, \tag{11}$$

$$\nu_{nf}\left(1+\frac{1}{\beta}\right)\left(\frac{d^4 g}{dy^4}\right) - \frac{\partial^3 g}{\partial y^2 \partial t} + k\left(f\frac{d^3 g}{dy^3} - \frac{dg}{dy}\frac{d^2 f}{dy^2}\right) = 0. \tag{12}$$

Integrating Eqs. (11) and (12) with respect to y and exhausting boundary conditions (10), we get

$$\nu_{nf}\left(1+\frac{1}{\beta}\right)\left(\frac{d^3 f}{dy^3}\right) - \frac{\pi J_0 M_0}{8\rho_f}\exp\left(-\frac{\pi}{a}y\right) + k\left(f\frac{d^2 f}{dy^2} - \frac{df}{dy}\frac{df}{dy}\right) = -k, \tag{13}$$

$$\nu_{nf}\left(1+\frac{1}{\beta}\right)\left(\frac{\partial^3 g}{\partial y^3}\right) - \frac{\partial^2 g}{\partial y \partial t} + k\left(f\frac{\partial^2 g}{\partial y^2} - \frac{\partial g}{\partial y}\frac{\partial f}{\partial y}\right) = 0. \tag{14}$$

We define

$$\begin{aligned} f(y) = \sqrt{\frac{\nu_f}{k}}F(\eta), \quad g(t,y) = \frac{\nu_f}{k}[G_o(\eta) + \varepsilon G_1(\eta)e^{i\tau}], \quad \eta = \sqrt{\frac{k}{\nu_f}}y, \Omega = \frac{w}{k}, \\ \tau = wt, \quad \varepsilon = \frac{U}{\sqrt{\nu_f k}}, \theta_o(y) + \varepsilon\theta_1(y) = \frac{T - T_\infty}{T_w - T_\infty}. \end{aligned} \tag{15}$$

In order to obtain the dimensionless form of Eqs. (5), (10), (13), and (14), we get

$$\left(\frac{\mu_{nf}}{\mu_f}\right)\left(\frac{\rho_f}{\rho_{nf}}\right)\left(1+\frac{1}{\beta}\right)(F''') - (F')^2 + FF'' + M\exp(-\omega\eta) = -1, \tag{16}$$

$$\left(\frac{\mu_{nf}}{\mu_f}\right)\left(\frac{\rho_f}{\rho_{nf}}\right)\left(1+\frac{1}{\beta}\right)(G_o''') - G_o'F' + G_o''F = 0, \tag{17}$$

$$\left(\frac{\mu_{nf}}{\mu_f}\right)\left(\frac{\rho_f}{\rho_{nf}}\right)\left(1+\frac{1}{\beta}\right)(G_1''') - G_1'F' + G_1''F - i\Omega G_1' = 0, \tag{18}$$

$$\frac{1}{pr}\frac{k_{nf}}{k_f}\theta_o'' + \frac{(\rho C_p)_S}{(\rho C_p)_f}F\theta_o' = 0, \tag{19}$$

$$\frac{k_{nf}}{k_f}\theta_1'' + pr\frac{(\rho C_p)_S}{(\rho C_p)_f}F\theta_1' - i\Omega pr\frac{(\rho C_p)_S}{(\rho C_p)_f}\theta_1 = 0, \tag{20}$$

Table 3. Verification of results for $f''(0)$.

M	[43]	Present Study
0.0	1.232593	1.232598
0.16	1.295369	1.295389
0.64	1.467975	1.467977
1.0	1.585329	1.585356

$$F'(\infty)=1, \quad F(0)=0, \quad F'(0)=0, \tag{21}$$

$$G_o'(\infty)=\gamma, \quad G_o(0)=0, \quad G_o'(0)=0, \tag{22}$$

$$G_1'(\infty)=\gamma, \quad G_1(0)=0, \quad G_1'(0)=0, \tag{23}$$

$$\theta_o(\infty)=0, \quad \theta_o(0)=1, \tag{24}$$

$$\theta_1(\infty)=0, \quad \theta_1(0)=1. \tag{25}$$

Where the Parameter $M=\frac{\pi J_0 M_0}{8\rho_f}$ is the modified Hartman number. For $M>0$, Lorentz force is +ve in x-direction, and -ve in x-direction for $M<0$. The thermal diffusivity of the nanofluid is discovered by α_{nf}, and $(\rho C_p)_{nf}$ the heat capacity of nanofluid, k_s, k_f the thermal conductivity of solid portions and base fluid υ_{nf} is kinematic viscosity of the nanofluid which is shown by [16],

$$\begin{aligned}
\mu_{nf} &= \frac{\mu_{nf}}{(1-\phi)^{2.5}\left[(1-\phi)\rho_f+\phi\rho_s\right]},\\
\rho_{nf} &= \phi\rho_s+(1-\phi)\rho_f,\\
\alpha_{nf} &= \frac{k_{nf}}{(\rho C_p)_{nf}},\\
(\rho C_p)_{nf} &= \phi(\rho C_p)_s+(1-\phi)(\rho C_p)_f,\\
\frac{k_{nf}}{k_f} &= \frac{-2\phi(k_s-k_f)+(k_s+2k_f)}{-\phi(k_s-k_f)+(k_s+2k_f)}.
\end{aligned} \tag{26}$$

The Skin friction number can be exalted as

$$C_f=\frac{\tau_w}{\frac{1}{2}\rho_f U_w^2}, \tag{27}$$

the shear stress is stated by

$$\tau_w=\left.\frac{\partial u}{\partial y}\right|_{y=0}. \tag{28}$$

Dimensionless form of Eq. (27), obtain

$$\frac{1}{2}Re_x C_f=\frac{1}{(1-\phi)^{2.5}}\left[\sqrt{Re}\,F''(0)+G''(0)+\varepsilon G''(0)e^{it}\right], \tag{29}$$

where $\mathrm{Re}=\frac{sx^2}{\upsilon_f}$, is the local Reynolds number.

The stream function is in dimensionless form

$$\psi^*=\frac{\psi}{\nu_f}=xF(\eta)+G(\eta). \tag{30}$$

Showing in Figure 1 an angle α with the plate is generating by the streamline and the slope of straight line can be found by setting $\psi^*=0$ as $\psi=\frac{1}{2}\gamma y^2+xy$ where $\eta=-\frac{2}{\gamma}x$ which gives slope $=-\frac{2}{\gamma}$. Hence the γ (shearing parameter) and α (impinging angle) relationship is

$$\alpha=\tan^{-1}\left(-\frac{2}{\gamma}\right). \tag{31}$$

The Nusslet number Nu is accessible as

$$Nu=\frac{xq_w}{k_f(T_w-T_\infty)}, \tag{32}$$

heat flux is calculated by

$$q_w=-k_{nf}\left.\frac{\partial T}{\partial y}\right|_{y=0}. \tag{33}$$

Dimensionless form of Eq. (32) given by

$$(Re_x)^{-1/2}Nu=\frac{k_{nf}}{k_f}\left[\theta'(0)+\varepsilon\theta'(0)e^{it}\right]. \tag{34}$$

4. Solution procedure

Numerical solution of the Eqs. (16), (17), (18), (19), and (20) is attained using BVP solution technique manufactured in Maple software. It can be predictable that foremost system (16–20) has one-way coupling i.e., $f(y)$ special effects $G_0(y), G_1(y)$, $\theta_0(y)$ and $\theta_1(y)$ but not vice versa. Also, for minor values of Ω, a series solution of Eqs. (18) and (20) has been gained, followed as

$$G_1(y)=\sum_{n=0}^{\infty}(i\Omega)^n\chi_n(y), \quad \textit{and} \quad \theta_1(y)=\sum_{n=0}^{\infty}(i\Omega)^n\vartheta_{1n}(y). \tag{35}$$

Taking the solution of real part only, as the form

$$G_1(y)=\chi_o(y)-\Omega^2\chi_2(y)+\Omega^4\chi_4(y)\cdots \tag{36}$$

Using Eq. (35) in Eqs. (18) and (23) we get

$$\left(\frac{\mu_{nf}}{\mu_f}\right)\left(\frac{\rho_f}{\rho_{nf}}\right)\left(1+\frac{1}{\beta}\right)\left(\chi_o'''\right)+\chi_o''F-\chi_o'F'=0, \tag{37}$$

$$\left(\frac{\mu_{nf}}{\mu_f}\right)\left(\frac{\rho_f}{\rho_{nf}}\right)\left(1+\frac{1}{\beta}\right)\left(\chi_n'''\right)+\chi_n''F-\chi_n'F'=0, \tag{38}$$

$$\chi_o'(0)=1, \quad \chi_o(0)=0, \quad \chi_o'(\infty)=1, \tag{39}$$

$$\chi_n'(0)=0, \quad \chi_n(0)=0, \quad \chi_n'(\infty)=0, \quad n=1,2,3\cdots \tag{40}$$

For Eq. (20), the series solution can also be explicated similarly.

$$\theta_1(y)=\sum_{n=0}^{\infty}(i\Omega)^n\vartheta_{1n}(y). \tag{41}$$

For minor values of Ω considering the real part only, we get

$$\theta_1(y)=\vartheta_{10}(y)-\Omega^2\vartheta_{12}(y)+\Omega^4\vartheta_{14}(y)\cdots \tag{42}$$

We have perceived that $\vartheta_{10}(y)=\theta_0(y)$ and solving $\theta_0(y)$ by direct integration we get

$$\theta_0(y)=\frac{J_{nf}(\infty,Pr)-J_{nf}(y,Pr)}{J_{nf}(\infty,Pr)}, \tag{43}$$

where

$$J_{nf}(y,Pr)=\int_0^y Exp\left(-Pr\frac{k_f}{k_{nf}}\frac{(\rho C_p)_{nf}}{(\rho C_p)_f}\int_0^s f(\eta)d\eta\right)ds. \tag{44}$$

Finally, the series form solution of the temperature Eq. (20) becomes

$$\frac{1}{pr}\frac{k_{nf}}{k_f}\vartheta''_{1n}+\frac{(\rho C_p)_{nf}}{(\rho C_p)_f}\left(f\vartheta'_{1n}-\vartheta_{1(n-1)}\right)=0, \tag{45}$$

$$\vartheta_{1n}(0)=1, \quad \vartheta_{1n}(\infty)=0, \quad n=1,2,3\cdots \tag{46}$$

The thermophysical properties of base fluid and nanoparticle are composed of [16].

5. Results and discussion

The above equations are solved by bvp4c method in maple and the current portion studies the performance of several flow parameters. Figure 2 expresses the performance for some values of dimensionless parameter W and Casson parameter β on velocity component $F'(\eta)$. When the values of W rise the velocity field reduces and the boundary layer also decrease. Figure 3 displays when β varies for two values and the modified Hartmann number M rises then the velocity field enhances and the thickness of the boundary layer declines. For $M>0$, Lorentz force is positive and negative for $M<0$ and M produces resistive type force in the boundary layer and that boundary layer reduces the motion of the fluid. If the Casson parameter β and modified Hartmann number M increase, then the velocity boundary layer viscosity develops solvent. On the other way, for Casson fluid it is noted that the velocity boundary layer viscosity is higher as compared to that of Newtonian fluid. Figure 4 explored when modified Hartmann number M vary for two values and the Casson parameter β is also rising then the boundary layer decreased and the velocity field increased and the behavior of the fluid convert Newtonian to non-Newtonian because it is noted that in non-Newtonian fluid the forces spread quickly then Newtonian fluid due to fact the radial velocity rises as β rises. The Lorentz force increases which attacks fluid flow by physically rising M. Hence velocity profile increases. Figure 5 displays the action for different values of β and W on velocity component $F'(\eta)$. When the values of W rises then the velocity field also raises and the boundary layer declines. Figures 6 and 7 discoveries the impact of the velocity profile $G_o(\eta)$ by changing β and M fixing the other parameters. Figure 8 shows the performance of the velocity component $G_o(\eta)$ by varies γ and M. Figure 9 shows that by adding nanoparticle the thermal boundary layer and the thermal conductivity escalate therefore the temperature profile enhances by increasing ϕ and β. It is clearly observed that the temperature profile is increasing the function of nanoparticle volume fraction. Figure 10 shows the action of velocity and velocity gradient $(f(y), f'(y), f''(y))$ is designated for $M=1.5$, $\beta=0.5$, $\gamma=0.5$, and it achieves the boundary conditions. Figure 11 shows the presence of the non-dimensional time t on $u(\eta,t)$ in a fixed frame of reference respectively. It is perceived that $u(\eta,t)$ is an oscillation. Figure 12 explored the disparity in Skin friction by changing γ. Figure 13 shows the effect of ϕ and Pr on Nusselt number. Increment arose due to increases of Pr. Figures 14, 15, 16, 17, 18, 19, 20, and 21 validate the impact of β and M on stream lines. Table 1 is made to examine the impact of γ and M on Skin friction and expresses the value of Skin friction increases due to increases in the value of the parameter. Table 2 is made to demonstrate the effect of γ and Pr on Nusselt number. This table illustrate when all parameters increases the value of Nusslet number also increases. Table 3 is made to validate the results.

6. Conclusion

The two-phase model for non-Newtonian nanofluid with Riga plate covering thermophoresis and Brownian motion effects is selected for investigation.

The resulting ideas are worth mentioning...

- The velocity field rises for $F'(\eta)$, and the velocity field rises and the boundary layer decreases.
- Temperature profile $\theta(y)$ drops with non-Newtonian parameter β, and ϕ.
- By increasing the M and thermal stratification the thermal boundary layer is dejected.

Declarations

Author contribution statement

Rizwana Rizwana: Conceived and designed the experiments; Wrote the paper.

Azad Hussain: Performed the experiments; Analyzed and interpreted the data.

S. Nadeem: Contributed reagents, materials, analysis tools or data.

Funding statement

This research did not receive any specific grant from funding agencies in the public, commercial, or not-for-profit sectors.

Competing interest statement

The authors declare no conflict of interest.

Additional information

No additional information is available for this paper.

References

[1] S.U. Choi, J.A. Eastman, Enhancing thermal Conductivity of Fluids with Nanoparticles (No. ANL/MSD/CP-84938; CONF-951135-29), Argonne National Lab., IL (United States), 1995.

[2] G. Hoghoughi, M. Izadi, H.F. Oztop, N. Abu-Hamdeh, Effect of geometrical parameters on natural convection in a porous undulant-wall enclosure saturated by a nanofluid using Buongiorno's model, J. Mol. Liq. 255 (2018) 148–159.

[3] Q. Yu, H. Xu, S. Liao, Analysis of mixed convection flow in an inclined lid-driven enclosure with Buongiorno's nanofluid model, Int. J. Heat Mass Tran. 126 (2018) 221–236.

[4] A. Purusothaman, K. Murugesan, A.J. Chamkha, 3D modeling of natural convective heat transfer from a varying rectangular heat generating source, J. Therm. Anal. Calorim. (2019) 1–12.

[5] A. Purusothaman, R.C.G. Sekar, K. Murugesan, Magnetic field and vibration effects on the onset of thermal convection in a grade fluid permeated anisotropic porous module, Therm. Sci. Eng. Prog. 10 (2019) 138–146.

[6] N. Shehzad, A. Zeeshan, R. Ellahi, K. Vafai, Convective heat transfer of nanofluid in a wavy channel: buongiorno's mathematical model, J. Mol. Liq. 222 (2016) 446–455.

[7] S. Nadeem, A.U. Khan, S. Saleem, A comparative analysis on different nanofluid models for the oscillatory stagnation point flow, Eur. Phys. J. Plus 131 (8) (2016) 261.

[8] M. Shen, L. Chen, M. Zhang, F. Liu, A renovated Buongiorno's model for unsteady Sisko nanofluid with fractional Cattaneo heat flux, Int. J. Heat Mass Tran. 126 (2018) 277–286.

[9] I. Khan, M.Y. Malik, A. Hussain, T. Salahuddin, Effect of homogenous-heterogeneous reactions on MHD Prandtl fluid flow over a stretching sheet, Res. Phys. 7 (2017) 4226–4231.

[10] H. Sadaf, M.U. Akbar, S. Nadeem, Induced magnetic field analysis for the peristaltic transport of non-Newtonian nanofluid in an annulus, Math. Comput. Simulat. 148 (2018) 16–36.

[11] K. Hiemenz, Die Grenzschicht an einem in den gleichformigen Flussigkeitsstrom eingetauchten geraden Kreiszylinder, Dinglers Polytech. J. 326 (1911) 321–324.

[12] R. Mehmood, S. Rana, N.S. Akbar, S. Nadeem, Non-aligned stagnation point flow of radiating Casson fluid over a stretching surface, Alexandria Eng. J. 57 (2) (2018) 939–946.

[13] S. Nadeem, R. Mehmood, N.S. Akbar, Optimized analytical solution for oblique flow of a Casson-nano fluid with convective boundary conditions, Int. J. Therm. Sci. 78 (2014) 90–100.

[14] M.M. Bhatti, M. Sheikholeslami, A. Shahid, M. Hassan, T. Abbas, Entropy Generation on the Interaction of Nanoparticles over a Stretched Surface with thermal Radiation. Colloids and Surfaces A: Physicochemical and Engineering Aspects, 2019.

[15] T. Weier, G. Gerbeth, G. Mutschke, E. Platacis, O. Lielausis, Experiments on cylinder wake stabilization in an electrolyte solution by means of electromagnetic

forces localized on the cylinder surface, Exp. Therm. Fluid Sci. 16 (1-2) (1998) 84–91.
[16] G. Rasool, T. Zhang, Characteristics of chemical reaction and convective boundary conditions in Powell-Eyring nanofluid flow along a radiative Riga plate, Heliyon 5 (4) (2019), e01479.
[17] A. Gailitis, On the possibility to reduce the hydrodynamic drag of a plate in an electrolyte, Appl. Magnetohydrodynamics, Rep. Inst. Phys. Riga 13 (1961) 143–146.
[18] A. Ahmad, S. Asghar, S. Afzal, Flow of nanofluid past a Riga plate, J. Magn. Magn Mater. 402 (2016) 44–48.
[19] R. Kumar, S. Sood, S.A. Shehzad, M. Sheikholeslami, Radiative heat transfer study for flow of non-Newtonian nanofluid past a Riga plate with variable thickness, J. Mol. Liq. 248 (2017) 143–152.
[20] R. Ahmad, M. Mustafa, M. Turkyilmazoglu, Buoyancy effects on nanofluid flow past a convectively heated vertical Riga-plate: a numerical study, Int. J. Heat Mass Tran. 111 (2017) 827–835.
[21] B.K. Mahatha, R. Nandkeolyar, G. Nagaraju, M. Das, MHD stagnation point flow of a nanofluid with velocity slip, non-linear radiation and Newtonian heating, Proc. Eng. 127 (2015) 1010–1017.
[22] Z. Iqbal, E. Azhar, Z. Mehmood, E.N. Maraj, Melting heat transport of nanofluidic problem over a Riga plate with erratic thickness: use of Keller Box scheme, Res. Phys. 7 (2017) 3648–3658.
[23] A. Naseem, A. Shafiq, L. Zhao, M.U. Farooq, Analytical investigation of third grade nanofluidic flow over a riga plate using Cattaneo-Christov model, Res. Phys. 9 (2018) 961–969.
[24] G. Nagaraju, M. Garvandha, Magnetohydrodynamic viscous fluid flow and heat transfer in a circular pipe under an externally applied constant suction, Heliyon 5 (2) (2019), e01281.
[25] G. Nagaraju, S. Jangili, J.V. Ramana Murthy, O.A. Beg, A. Kadir, Second law analysis of flow in a circular pipe with uniform suction and magnetic field effects, J. Heat Tran. 141 (1) (2019).
[26] M.M. Bhatti, R. Ellahi, A. Zeeshan, M. Marin, N. Ijaz, Numerical study of heat transfer and Hall current impact on peristaltic propulsion of particle-fluid suspension with compliant wall properties, Mod. Phys. Lett. B 33 (35) (2019) 1950439.
[27] M.M. Bhatti, A. Shahid, T. Abbas, S.Z. Alamri, R. Ellahi, Study of activation energy on the movement of gyrotactic microorganism in a magnetized nanofluids past a porous plate, Processes 8 (3) (2020) 328.